A New Three-Dimensional Exponential Material Model of the Coronary Arterial Wall to Include Shear Stress Due to Torsion

J. Scott Van Epps

David A. Vorp[1]
e-mail: vorpda@upmc.edu

Department of Surgery,
Department of Bioengineering,
the McGowan Institute for Regenerative Medicine,
and the Center for Vascular Remodeling and Regeneration,
University of Pittsburgh,
Pittsburgh, PA 15219

The biomechanical milieu of the coronary arteries is unique in that they experience mechanical deformations of twisting, bending, and stretching due to their tethering to the epicardial surface. Spatial variations in stresses caused by these deformations could account for the heterogeneity of atherosclerotic plaques within the coronary tree. The goal of this work was to utilize previously reported shear moduli to calculate a shear strain parameter for a Fung-type exponential model of the arterial wall and determine if this single constant can account for the observed behavior of arterial segments under torsion. A Fung-type exponential strain-energy function was adapted to include a torsional shear strain term. The material parameter for this term was determined from previously published data describing the relationship between shear modulus and circumferential stress and longitudinal stretch ratio. Values for the shear strain parameter were determined for three geometries representing the mean porcine left anterior descending coronary artery dimensions plus or minus one standard deviation. Finite element simulation of triaxial biomechanical testing was then used to validate the model. The mean value calculated for the shear strain parameter was 0.0759 ± 0.0009 ($N = 3$ geometries). In silico triaxial experiments demonstrated that the shear modulus is directly proportional to the applied pressure at a constant longitudinal stretch ratio and to the stretch ratio at a constant pressure. Shear moduli determined from these simulations showed excellent agreement to shear moduli reported in literature. Previously published models describing the torsional shear behavior of porcine coronary arteries require a total of six independent constants. We have reduced that description into a single parameter in a Fung-type exponential strain-energy model. This model will aid in the estimation of wall stress distributions of vascular segments undergoing torsion, as such information could provide insight into the role of mechanical stimuli in the localization of atherosclerotic plaque formation. [DOI: 10.1115/1.2948396]

Keywords: biomechanics, coronary arteries, torsion, twisting, constitutive equation, material properties, exponential strain-energy function

1 Introduction

One of the primary aims in the treatment and prevention of atherosclerosis is the reduction of risk factors (e.g., dyslipidemia, hypertension, smoking, and diabetes) known to be linked with increased incidence of disease [1]. This approach has led to only modest reductions in mortality [2]. Since risk factors are systemic in nature, and the distribution of atherosclerotic plaques is highly localized and heterogeneous [1], other factors likely influence the localization of atherogenesis. The complex and spatially variable biomechanical milieu is thought to mediate location specific atheroprotection or susceptibility [3,4]. Fluid shear stress due to dynamic blood flow [5–11] as well as solid stress due to vessel wall distensions [12–16] have been correlated with lesion localization.

Most of the research relating local biomechanical stimuli to atherogenic localization has focused specifically on the fluid-induced shear stresses. However, there is increasing evidence that mural stresses within the vessel wall exert additional influence on the atherogenic potential for a given location [4]. For instance, the ostia of major vessel branches, the aortic arch, and the bifurcation of the aorta and carotid arteries are the areas predicted to have increased intramural stress [15,16]. This presence of altered mural stresses confounds the assertion that fluid stresses are the sole contributor to the increased prevalence of atherosclerosis in these areas [5–11]. Furthermore, the absence of atherosclerotic lesions in the intramyocardial arteries and the intraosseous portions of the vertebral arteries corresponds to decreased mural stress provided by the external support of the myocardium and vertebrae, respectively [15]. The protective effect of reduced intramural stress was demonstrated whereby external casts that reduce circumferential expansion of arteries reduced the development of atherosclerosis in cholesterol-fed rabbits [13].

Further evidence for role of intramural stresses in the localization of atherosclerosis comes from examination of the coronary arterial bed. The coronary arteries are unique in that they are particularly susceptible to atherogenesis, with fatty streaks appearing early during childhood [17]. In addition, the coronary arteries experience dynamic mechanical deformations such as flexure, stretching, and twisting, since they are tethered to a beating heart [18–22]. There is sufficient variability of these motion parameters along the length of a given vessel, between the right and left coronary arteries, and between individuals to account for the extreme variability in lesion localization and patient specific suscep-

[1]Corresponding author.

Contributed by the Bioengineering Division of ASME for publication in the JOURNAL OF BIOMECHANICAL ENGINEERING. Manuscript received June 28, 2007; final manuscript received January 21, 2008; published online July 10, 2008. Review conducted by Andrew D. McCulloch. Paper presented at the 2007 Summer Bioengineering Conference (SBC2007), Keystone, CO, June 20–24, 2007.

tibility [18,19]. Furthermore, Stein et al. demonstrated that areas of increased flexure angle, and the resulting increased mural stresses, were correlated with increased lesion progression [12].

Cyclic twisting of the coronary arteries and the resulting shear stresses within their walls is another potential modulator of atherogenesis. Biplane cineangiographic reconstruction studies have demonstrated that the coronary arteries experience as much as 20 deg of torsion during a cardiac cycle [22]. Given the sensitivity of vascular cells (endothelial and smooth muscle) to various deformation and fluid-induced mechanical stimuli [4,23], this motion could play a significant role in the mechanopathobiology of atherogenesis. However, to date, there has been little investigation on the contribution of torsion to the total stress distribution within the vessel wall and therefore its role in the localization of atherosclerosis.

Finite element analysis is the preferred method for estimation of stress distributions in bodies under various loading conditions, including torsion. Finite element analysis, however, requires detailed knowledge of the material properties of the body in question. In the case of torsion, shear moduli due to twisting have been determined for pig coronary arteries [24] and rat aortas [25]. However, these moduli are not constant, varying with the longitudinal stretch ratio and the applied internal pressure. Therefore, in the case of the porcine coronary arteries, a family of equations was used to describe the relationship between shear modulus and stretch ratio and internal pressure [24]. However, this material description is not a strain-energy model and therefore not conducive to finite element analysis. In order to develop a finite element simulation of the arterial wall under torsion, a strain-energy model that incorporates this relationship between shear modulus and the other mechanical stimuli is required.

The goal of this work was to utilize previously reported shear moduli to calculate a shear strain parameter in a Fung-type exponential strain-energy model of the arterial wall and determine if this single constant can account for the observed behavior of arterial segments under torsion.

2 Methods

2.1 Biomechanical Principles. In this analysis, the coronary artery is assumed to be a straight cylinder with a circular cross section (Fig. 1(*A*)). Therefore, the dimensions of a segment of this artery can be defined by the length (L), the inner radius (r_i), and the outer radius (r_o). It is acted upon by a pressure (P) (i.e., blood pressure), a longitudinal tension which generates a stretch ratio (λ), and a torque (T), which causes the vessel to twist by an angle (θ). As previously demonstrated, the zero-stress state (the configuration in which all loads are zero) of an artery is determined by making a radial cut in an arterial ring, allowing the ring to open into a sector [26,27]. The inner (R_i) and outer radii (R_o) and opening angle (Φ) of that sector represent the zero-stress or reference configuration (Fig. 1(*B*)).

The deformation gradient $\mathbf{F}$ of an intact, loaded, arterial segment would be

$$\mathbf{F} = \begin{bmatrix} \frac{\partial r}{\partial R} & 0 & 0 \\ 0 & \frac{\pi r}{\Phi R} & r\gamma \\ 0 & 0 & \lambda \end{bmatrix} \tag{1}$$

where γ is the twist per unit length or θ/L [28]. Assuming that arterial tissue is incompressible requires that the determinant of $\mathbf{F}$ is 1. Thus,

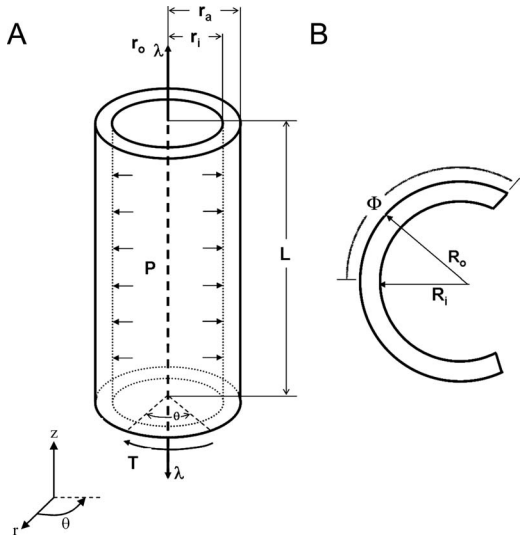

Fig. 1 (*A*) Schematic of an arterial segment of length *L* and inner and outer radii r_i and r_o, respectively, acted upon by a longitudinal stretch λ, an intraluminal pressure *P*, and a torque *T*, which generates a twist angle θ. (*B*) Schematic of a sector of an arterial ring with inner and outer radii R_i and R_o, respectively, and an opening angle Φ.

$$\frac{\partial r}{\partial R} = \frac{\Phi R}{\pi r \lambda} \tag{2}$$

The deformation of a given point in this arterial segment can be characterized by Lagrangian Green's strain tensor ($\mathbf{E}$), which is given by

$$\mathbf{E} = \frac{1}{2}(\mathbf{F}^T \cdot \mathbf{F} - \mathbf{I}) = \frac{1}{2}\begin{pmatrix} \left(\frac{\Phi R}{\pi r \lambda}\right)^2 - 1 & 0 & 0 \\ 0 & \left(\frac{\pi r}{\Phi R}\right)^2 - 1 & \frac{r^2 \pi \gamma}{\Phi R} \\ 0 & \frac{r^2 \pi \gamma}{\Phi R} & r^2\gamma^2 + \lambda^2 - 1 \end{pmatrix} \tag{3}$$

where $\mathbf{I}$ is the identity matrix [28].

Humphrey described a generalized form of a strain-energy function to describe the elasticity of finite deformations in arterial tissue as follows:

$$W = \tfrac{1}{2}c_0(e^Q - 1) \tag{4}$$

where

$$Q = c_1E_r^2 + c_2E_\theta^2 + c_3E_z^2 + 2c_4E_\theta E_r + 2c_5E_\theta E_z + 2c_6E_zE_r + c_7(E_{\theta z}^2 + E_{z\theta}^2) + c_8(E_{rz}^2 + E_{zr}^2) + c_9(E_{\theta r}^2 + E_{r\theta}^2) \tag{5}$$

E_r, E_θ, and E_z are the principal components and $E_{\theta z}$, etc., are the shear components of the Green's strain tensor shown in Eq. (3) [28]. Note that a more specific form of this model was originally put forth by Chuong and Fung [29]. They assumed a cylindrical, orthotropic, material symmetry and therefore determined constants for only the first six terms in Eq. (5) [29].

The loading case described in Eq. (3) allows simplification of the general exponential strain-energy function in Eqs. (4) and (5). Specifically, E_{rz}, E_{zr}, $E_{\theta r}$, and $E_{r\theta}$ are zero. Also, E is symmetric (i.e., $E=E^T$), which makes $E_{\theta Z}=E_{Z\theta}$. Therefore, the simplified form of Q becomes

$$Q = c_1E_r^2 + c_2E_\theta^2 + c_3E_z^2 + 2c_4E_\theta E_r + 2c_5E_\theta E_z + 2c_6E_zE_r + 2c_7E_{\theta z}^2 \tag{6}$$

The Cauchy stress tensor ($\boldsymbol{\sigma}$) can then be determined from the strain-energy function via

$$\boldsymbol{\sigma} = -p\mathbf{I} + \mathbf{F} \cdot \frac{\partial W}{\partial \mathbf{E}} \cdot \mathbf{F}^T \tag{7}$$

where p is the Lagrangian multiplier.

2.2 Experimental Data. Values for parameters c_0–c_6 have been previously determined for porcine coronary arteries [30]. No values have been reported for the proposed parameter c_7, but the work by Lu et al. describing the shear modulus properties of porcine coronary arteries provide the necessary information to determine its value [24]. They demonstrated that the torque required to twist an artery varied linearly with γ. Therefore, the relationship between torsion shear stress and shear strain can be described by

$$\overline{\sigma_{\theta z}} = Gr\gamma \tag{8}$$

where G is the shear modulus. G was found to be linearly proportional to the mean circumferential stress, such that

$$G = \alpha + \beta\overline{\sigma_\theta} \tag{9}$$

where $\overline{\sigma_\theta}$ is determined from the law of Laplace [24]. The linear constants (α and β) were found to depend on the longitudinal stretch ratio λ. The result was a family of linear functions describing the relationship between G, λ, and $\overline{\sigma_\theta}$.

2.3 Derivation of an Expression for c_7. While these previous experiments by Lu et al. [24] provide the necessary data for developing a finite element model of arterial segments under torsion, the form of the relationship is not conducive for finite element analysis. Ideally, the relationship would be encompassed in the strain-energy function, specifically in the value of the parameter c_7. To do this, we derived the Cauchy torsion shear stress component from Eqs. (3), (4), (6), and (7) to be

$$\sigma_{\theta z} = \left(\frac{\pi r\lambda}{\Phi R}\right)\frac{\partial W}{\partial E_{\theta z}} + r\gamma\lambda\frac{\partial W}{\partial E_z} \tag{10}$$

Evaluating the derivatives yields

$$\sigma_{\theta z} = c_0c_7\left(\frac{\pi r}{\Phi R}\right)^2 r\gamma\lambda e^Q + c_0(c_5E_\theta + c_6E_r + c_3E_z)r\gamma\lambda e^Q \tag{11}$$

Setting Eq. (11) equal to expression (8) derived by Lu et al. [24] gives

$$(\alpha + \beta\overline{\sigma_\theta}) = c_0c_7\left(\frac{\pi r}{\Phi R}\right)^2 \lambda e^Q + c_0(c_5E_\theta + c_6E_r + c_3E_z)\lambda e^Q \tag{12}$$

Solving for c_7 gives

$$c_7 = \left(\frac{\Phi R}{\pi r}\right)^2\left[\frac{(\alpha + \beta\overline{\sigma_\theta})}{c_0\lambda e^Q} - (c_5E_\theta + c_6E_r + c_3E_z)\right] \tag{13}$$

Note that Eq. (13) is not a closed form solution because c_7 appears in the expression for Q (see Eq. (6)). However, it was assumed that c_7 makes a negligible contribution to Q and therefore Q was calculated without the c_7 term in the evaluation of Eq. (13). The validity of this assumption was confirmed once the values of c_7 were determined.

2.4 Finite Element Analysis-Based Calculation of c_7. Based on Eq. (13), the data on the strain state of an arterial segment under circumferential (pressure) and longitudinal (stretch) loads are required to calculate c_7. This information was obtained by finite element analysis using ABAQUS V6.5. The user-defined subroutine UMAT was used for incorporation of custom material properties; i.e., W given by Eqs. (4) and (6) (see the Appendix).

Table 1 Porcine LAD dimensions

	Small	Medium	Large
Inner radius (mm)	0.817	0.963	1.108
Outer radius (mm)	1.047	1.219	1.390
Wall thickness (μm)	230	256	282

The parameters used in Eq. (6) were previously determined by Wang et al. [30] for intact porcine left anterior descending (LAD) artery: c_0=8.92 kPa, c_1=0.55, c_2=1.25, c_3=2.46, c_4=0.08, c_5=0.36, and c_6=0.06. The specific gravity was assumed to be 1.0 and the arterial tissue was assumed to be incompressible. This constraint was applied by the use of the penalty function

$$\varphi(J) = (J-1)^2 \tag{14}$$

where J is the determinant of the deformation gradient F. This constraint was used in place of the Lagrangian multiplier in Eq. (7) making the Cauchy stress

$$\boldsymbol{\sigma} = \mathbf{F} \cdot \frac{\partial W}{\partial \mathbf{E}} \cdot \mathbf{F}^T + \eta\frac{\partial \varphi}{\partial \varepsilon} \tag{15}$$

where $\boldsymbol{\varepsilon}$ is the logarithmic strain tensor and η is the penalty parameter. Incompressibility was maintained with $\eta = 10^6$. Three different geometries representing the mean (medium) porcine LAD dimensions plus (large) or minus (small) one standard deviation (Table 1) [31] were constructed and meshed using eight-node generalized biquadratic axisymmetric quadrilateral hybrid elements. All geometries had the same length (20 mm) and opening angle (2.97 rad).

The analyses for the calculation of c_7 were performed in two static loading steps. The first step was a linear ramp in the longitudinal stretch until the desired λ was achieved. The second was a linear ramp in pressure from 0 kPa to 16 kPa. The resulting inner and outer radii were computed during this pressurization step and used in the calculation of c_7 at the 21 combinations of applied pressure and stretch. It should be noted that by using a static analysis, all inertial effects were ignored.

Mean values for the parameter c_7 of the arterial segment were determined at pressures of 0 kPa, 3 kPa, 5 kPa, 8 kPa, 10.7 kPa, 13.3 kPa, and 16 kPa (corresponding to 0 mm Hg, 22.5 mm Hg, 60 mm Hg, 80 mm Hg, 100 mm Hg, and 120 mm Hg, respectively) with longitudinal stretch ratios of 1.2, 1.3, and 1.4; thus generating 21 distinct values, which were then averaged. This was repeated for each of the three geometries in Table 1.

2.5 In Silico Triaxial Experiments. Each value determined for c_7 was validated through in silico simulation of the triaxial experiments performed by Lu et al. [24]. As before, finite element analysis was performed using ABAQUS V6.5 with the UMAT (see the Appendix) user-defined subroutine on the three geometries indicated in Table 1. However, in this case, the strain-energy function utilized by UMAT was that defined in Eqs. (4) and (6) incorporating the newly calculated value for c_7. The simulated experiments had three loading steps (Fig. 2). There was a sequential linear ramp first in stretch and then in pressure to desired values. Following this, one end of the vessel segment was fixed in position while a clockwise circumferential displacement was applied to the other end, generating a twist angle of −25 deg. The displacement was then reversed; i.e., a counterclockwise circumferential displacement was applied until the twist angle reached 25 deg. The shear stress ($\sigma_{\theta Z}$) evaluated at the nodes of the end being displaced circumferentially was recorded throughout the twist loading cycle. These values were used to calculate the torque (T) required to achieve this twist via

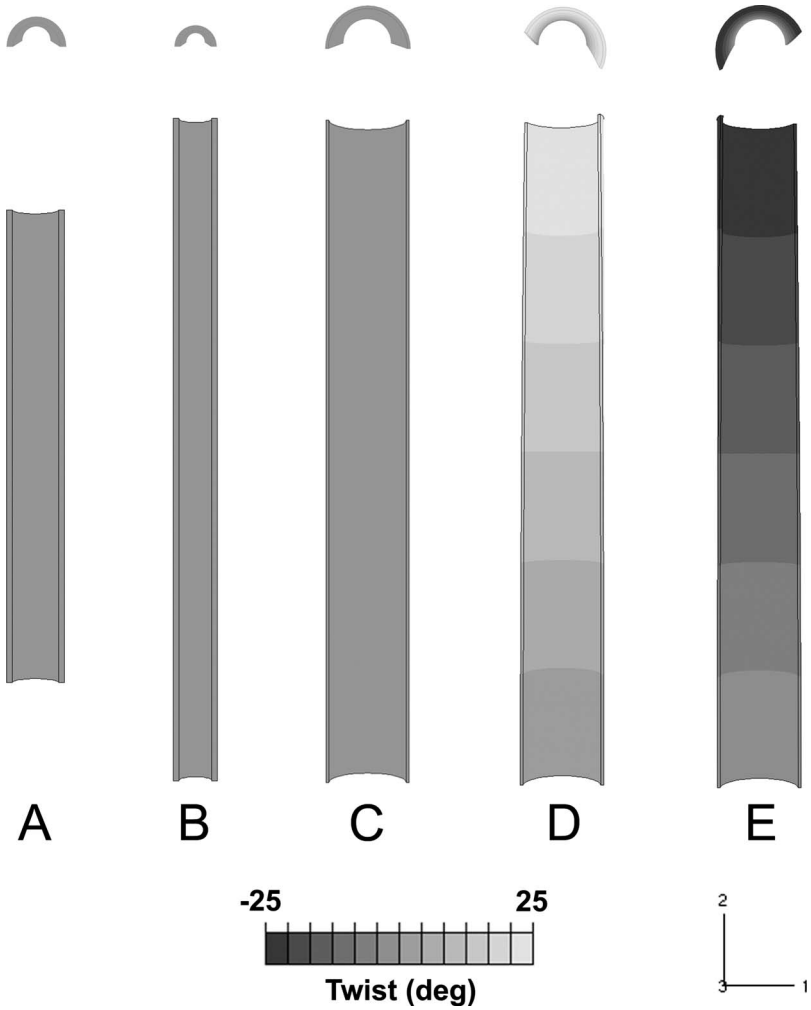

Fig. 2 In silico triaxial experimental protocol demonstrated by a representative vessel geometry. Two views are shown of a hemivessel at each step with an angle of twist plotted as gray scale. An end view (top) and a side view into the open end of the hemivessel (bottom). (*A*) Vessel segment in the unloaded configuration; (*B*) stretched to the desired λ; (*C*) pressurized to the desired *P*; (*D*) twisted on the upper end by $\theta = -25$ deg; (*E*) and twisted in the opposite direction, $\theta = 25$ deg.

$$T = 2\pi \int_{r_i}^{r_o} \sigma_{\theta z} r^2 dr \tag{16}$$

This integral was estimated via the trapezoid rule evaluated at the finite element nodes. Substituting the relationship between shear stress and shear modulus (see Eq. (8)) determined by Lu et al. [24] and evaluating the integral in Eq. (16) give

$$T = GK\gamma \tag{17}$$

where K is the polar moment of inertia given by

$$K = \frac{\pi}{2}(r_o^4 - r_i^4) \tag{18}$$

Plots of torque (T) versus polar moment of inertia times the twist per unit length ($K\gamma$) were generated for each combination of stretch ratio and pressure. The shear modulus (G) was then determined from the slope of these lines and compared to the moduli determined experimentally by Lu et al. [24].

3 Results

3.1 Values for the Parameter c_7. The inner and outer radii computed via finite element analysis for each of the three porcine LAD geometries in Table 1 for a given longitudinal stretch and pressure combination are shown in Fig. 3. The average values of c_7 calculated according to Eq. (13) for each longitudinal stretch and pressure combination for a given geometry are shown in Fig. 4. The average value for c_7 across the three geometries was 0.0759 ± 0.0009 (mean $\pm$ standard deviation).

3.2 In Silico Triaxial Experiments. Incorporation of the average value for the c_7 term into the finite element simulation employing the exponential strain-energy function defined by Eqs. (4) and (6) generated the family of linear functions between torque and polar moment of inertia times twist per unit length shown in Fig. 5. A comparison of the family of linear functions used to describe the shear moduli by Lu et al. [24] and the single exponential model with the c_7 term shows close agreement ($R^2 > 0.98$) independent of the vessel segment geometry (Fig. 6).

3.3 Validation of Assumptions and Simulation Quality.

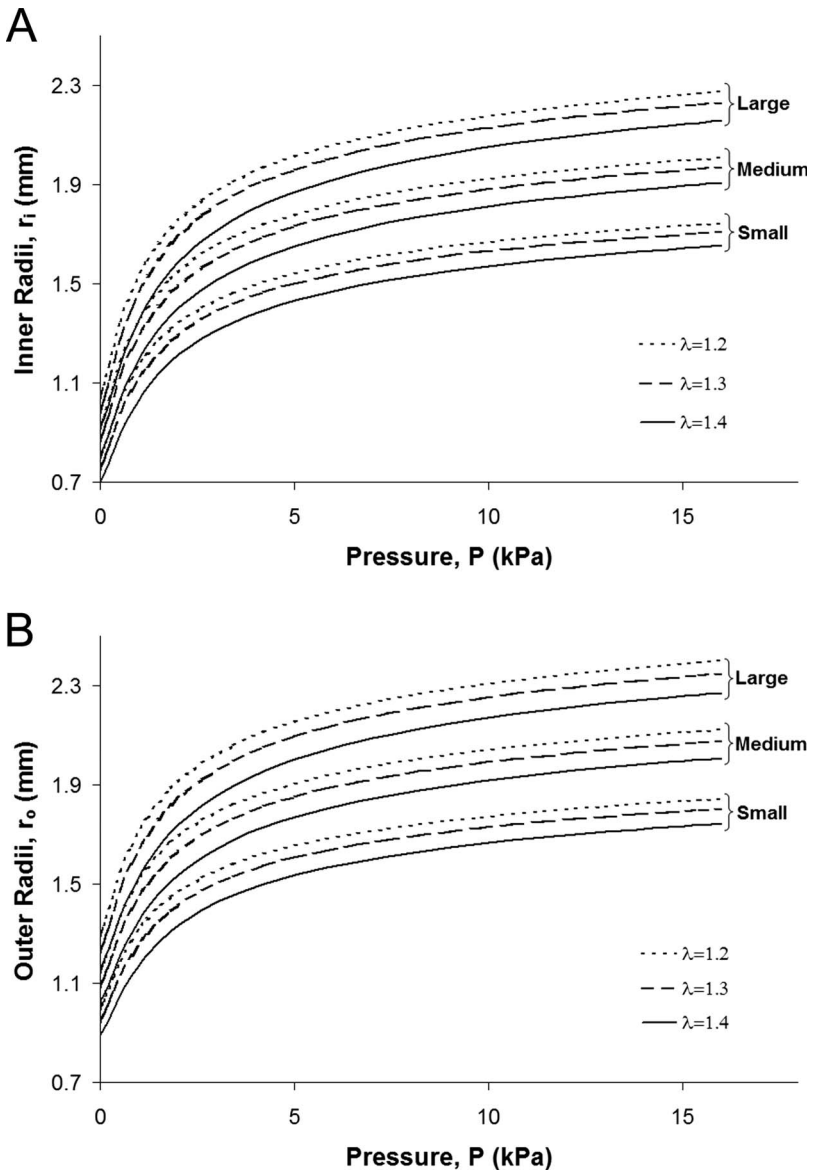

Fig. 3 Plots of computed inner (*A*) and outer (*B*) radii versus pressure for the three porcine LAD geometries (small, medium, and large) at stretch ratios of 1.2, 1.3, and 1.4

The difference between the values of Q at the maximum and minimum loading conditions of the mean LAD geometry with and without the c_7 term was found to be less than 0.02%, suggesting that c_7 does indeed have a negligible contribution to Q. The determinant (J) of the deformation gradient was monitored throughout the analysis and found to range from 0.9998 to 1.0004, suggesting that incompressibility assumption was met.

Valid finite element analysis requires that the results be independent of the mesh size. To ensure mesh independence, the shear stresses $\sigma_{\theta Z}$ at the end nodes used in the evaluation of the torque from Eq. (16) were determined to be nearly the same for three different mesh densities (Fig. 7). All reported results utilized the medium mesh density.

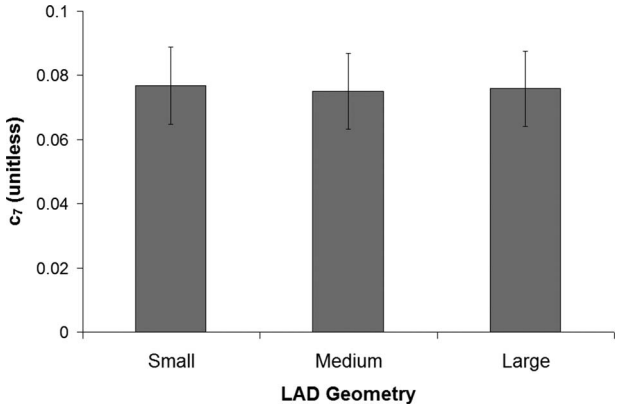

Fig. 4 Calculated values for the parameter c_7 for each porcine LAD geometry (small, medium, and large). The bars represent the average value from each combination of pressure (0 kPa, 3 kPa, 5 kPa, 8 kPa, 10.7 kPa, 13.3 kPa, and 16 kPa) and stretch ratio (1.2, 1.3, and 1.4), a total of 21 combinations. The error bars represent the standard error of the mean.

4 Discussion

Characterization of the mechanical stress distribution in the coronary arterial bed could provide insight into the mechanisms' underlying atherosclerotic lesion localization. The torsion shear component of that stress distribution has been understudied due to

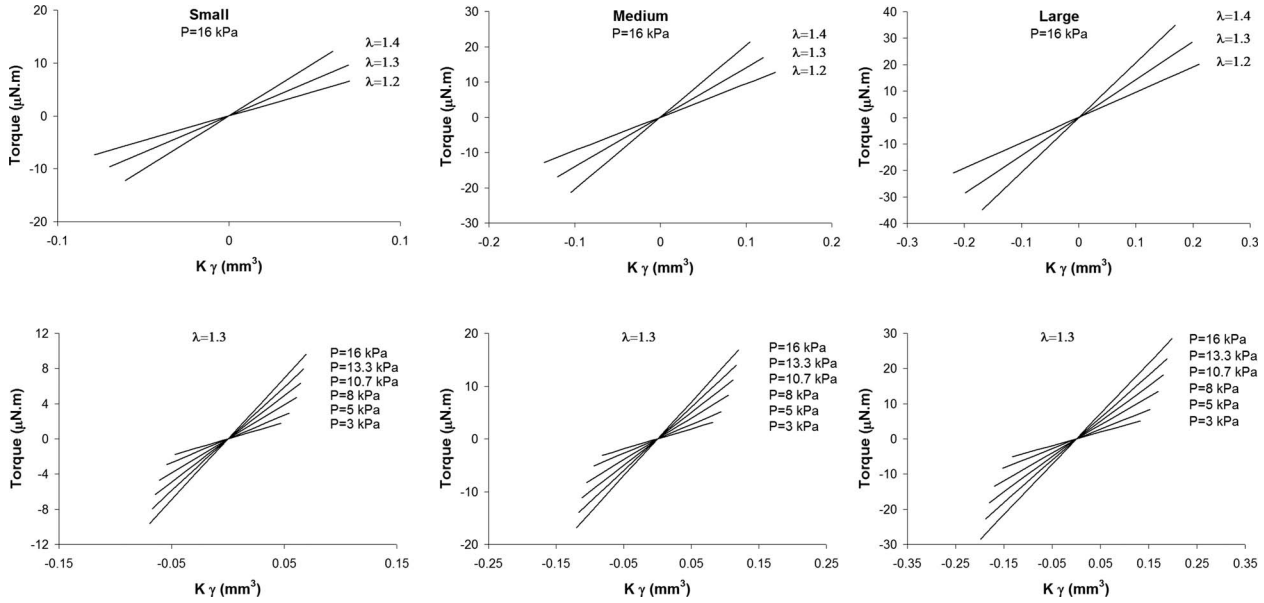

Fig. 5 Plots of torque versus polar moment of inertia (γ) for various stretch ratios at constant pressure (top) and various pressures at constant stretch ratio (bottom) for each of the three vessel geometries (small, medium, and large)

the lack of a well-defined material model of the arterial wall that includes this component of mechanical deformation. The benefits of this work to that end are multifold. Lu et al. previously used triaxial mechanical testing to determine a family of linear functions for the shear modulus of porcine coronary arteries [24]. In all, six linear parameters were required to describe the torsion shear properties of one porcine coronary artery. While this model provided a continuous distribution for shear modulus with respect to circumferential stress, it could only describe a discrete distribution with respect to longitudinal stretch ratio. That is, if the vessel of interest had a stretch ratio between 1.2 and 1.3, a potentially nonlinear interpolation would be necessary. The model we propose here solves that problem by providing a single constant that characterizes the entire physiologic spectrum of shear moduli for pressures between 0 mm Hg and 120 mm Hg and longitudinal stretch ratios between 1.2 and 1.4. In addition, a material model that is invertible, such as the one described by the Fung-type exponential strain-energy function used here, allows for its use in finite element analysis. This is significant in that it allows one to characterize the stress distribution in arterial tissue under torsion.

In silico simulation of triaxial experiments demonstrated that this single parameter captures the dependence of torsion shear stress on circumferential and longitudinal stresses. Furthermore, the values of the shear modulus calculated for the porcine LAD from this study agreed with those published previously [24]. While this study focused specifically on the porcine LAD, shear moduli data have been reported for the right coronary artery in the pig [24] and the aorta in the rat [25]. This methodology could easily be employed to determine the value of c_7 for those particular vessels as well.

The validity of our methodology can be evaluated with a few key observations. The first is that the value of c_7 is independent of the vessel segment size. Second, the value of c_7 is small relative to other parameters in the model. In fact, it is small enough to be negligible in the calculation of the exponent Q, which is appropriate, since the twisting deformation is expected to have a very small contribution to the other nontorsion stresses in the arterial wall. Third, the results are independent of mesh density indicating appropriate mesh size and boundary conditions in the finite element analysis.

Like all simulation studies, the results are limited by the assumptions made. First, the analysis assumes an axisymmetric geometry with constant diameter and wall thickness over the length. However, the coronary arteries have a complex geometry with significant branching and a continuous distribution of both diameter and wall thickness over the length [32]. Furthermore, the zero-stress state, characterized by the opening angle, also varies longitudinally [32]. For this analysis, the dimensions were assumed to be constant and equal to those of the porcine left coronary artery prior to the first major branch. The straight, axisymmetric assumption has been previously employed by Lu et al. as well as others to evaluate the torsion shear properties of vascular tissue [24,25]. Our results can therefore be interpreted with respect to these previous studies. Second, extrapolation of our results beyond the conditions tested should be performed with care. Residual analysis demonstrates an increase in error toward the ends of the testing range, indicating that this model may not be valid at pressures above 120 mm Hg and stretch ratios below 1.2 or above 1.4. This limited range of stretch ratios should not detract from the overall utility of the model since the stretch ratio is unlikely to vary outside this range specifically during torsional loading in vivo. The nonlinear effects of longitudinal stretch independent of torsional shear are already included in the original Fung model that formed the basis of the model described here. A higher order model may be required to characterize the shear stress behavior under these more extreme loading conditions. Third, this model was developed from the stress-strain state of blood vessels at a single point in time without prior knowledge of loading history. Therefore, it cannot provide information about remodeling.

In summary, we condensed the description of the torsion shear properties of the porcine LAD from a family of linear functions to a single parameter added to a well-validated Fung-type exponential material model. Finite element analyses utilizing this model can more accurately predict the various components of stress within the wall of vessels undergoing torsional deformation, such as the coronary arteries. Such computational modeling using accurate material models could aid in determining the mechanistic link between biomechanical stimuli and the localization of atherogenesis.

Acknowledgment

This work was funded in part by the National Institutes of Health, Fellowship No. F31 EB004718 and the University of

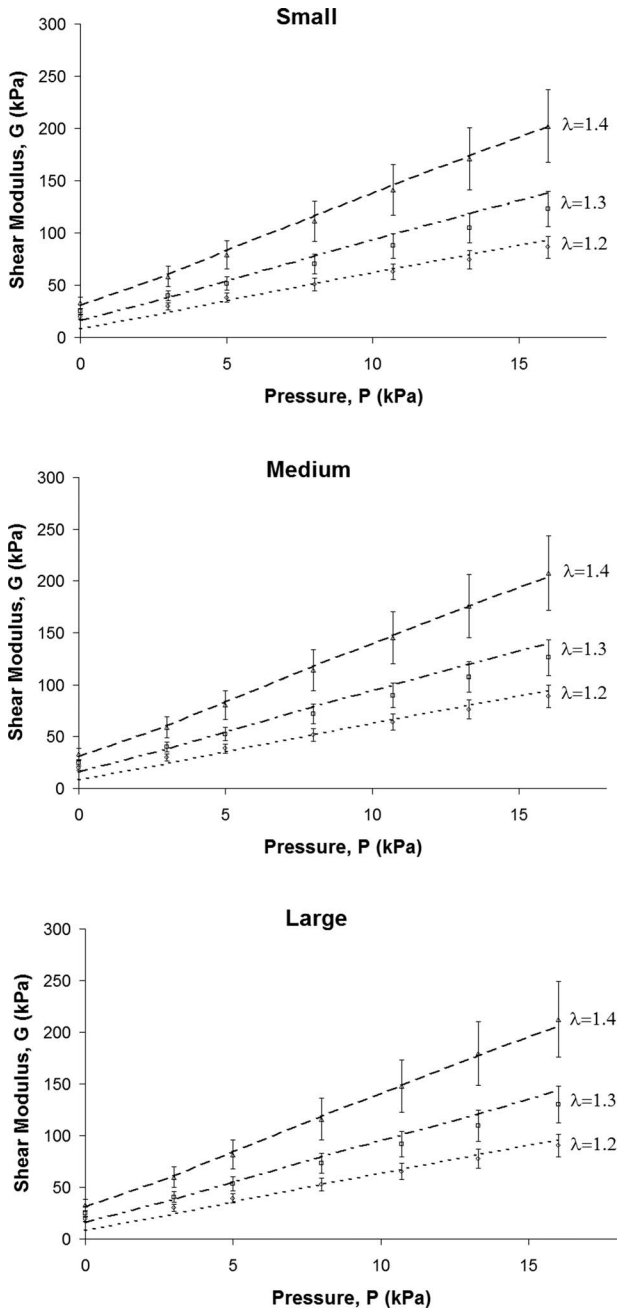

Fig. 6 Shear modulus (*G*) as a function of pressure for various stretch ratios for each of the three vessel geometries (small, medium, and large). Individual points represent shear moduli determined by linear functions of mean circumferential wall stress from Lu et al. [24]. The error bars represent a 95% confidence interval. The lines represent shear moduli predicted from the in silico triaxial experiments using *W* defined by Eqs. (4) and (6); i.e., including the shear strain term (c_7=0.0759).

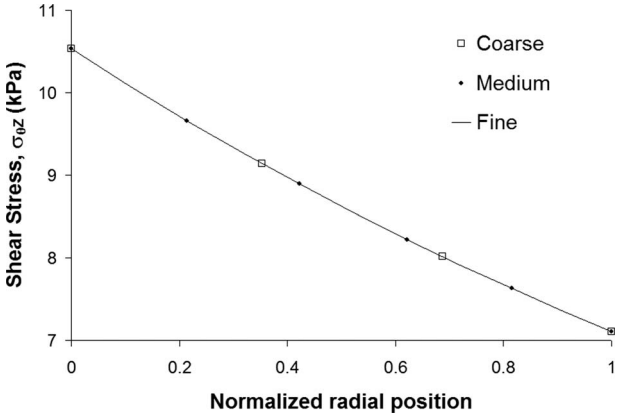

Fig. 7 Mesh independence analysis. The radial distribution of shear stress ($\sigma_{\theta z}$) for the nodes at the twist end of the vessel is shown for three different mesh densities (coarse, medium, and fine).

Pittsburgh Center for Vascular Remodeling and Regeneration.

Appendix: Development of Custom UMAT File for ABAQUS V6.5

ABAQUS V6.5 provides the user-defined subroutine, UMAT, for custom definition of material constitutive properties. This subroutine can be used to update the stresses and Jacobian matrix from the provided deformation gradient at each increment. UMAT utilizes the Cauchy "true" definition of stress and defines the Jacobian matrix as

$$\frac{\partial \Delta \boldsymbol{\sigma}}{\partial \Delta \boldsymbol{\varepsilon}} \tag{A1}$$

where $\boldsymbol{\varepsilon}$ is the logarithmic strain tensor defined by

$$\boldsymbol{\varepsilon} = \ln \mathbf{F} \tag{A2}$$

Implementation of this subroutine for incorporation of the strain-energy model described in this study required two expressions. First, an expression for the Cauchy stress tensor was derived as a function of the deformation gradient (see Eqs. (1)–(7)). Second, the Jacobian matrix was determined from the Cauchy stress tensor. Since the strain-energy function is given in terms of Green's strain, the Cauchy stress tensor is also in terms of Green's strain. The Jacobian matrix with respect to the logarithmic strain can be determined by application of the chain rule

$$\frac{\partial \boldsymbol{\sigma}}{\partial \boldsymbol{\varepsilon}} = \frac{\partial \mathbf{E}}{\partial \boldsymbol{\varepsilon}} \frac{\partial \boldsymbol{\sigma}}{\partial \mathbf{E}}$$

$$\frac{\partial \boldsymbol{\sigma}}{\partial \boldsymbol{\varepsilon}} = (\mathbf{I} + 2\mathbf{E}) \frac{\partial \boldsymbol{\sigma}}{\partial \mathbf{E}} \tag{A3}$$

Since this was an axisymmetric analysis, it was assumed that $E_{\theta z}$ is the predominant shear strain and that the other shear strains (E_{rz} and $E_{\theta r}$) were negligible. To enforce this constraint, two additional terms had to be added to the exponent Q in the strain-energy function such that

$$Q = c_1 E_r^2 + c_2 E_\theta^2 + c_3 E_z^2 + 2(c_4 E_\theta E_r + c_5 E_\theta E_z + c_6 E_z E_r + c_7 E_{\theta z}^2 + c_8 E_{rz}^2 + c_9 E_{\theta r}^2) \tag{A4}$$

These terms were added to aid in computational stability and force a near zero shear strain in the r-z and r-θ planes. Therefore, the parameters c_8 and c_9 were not true material constants. Rather, their values were arbitrarily chosen to be large enough to prevent shear deformations in the respective planes. Zhang et al. employed a similar technique in their axisymmetric fluid-structure analysis of the effect of surrounding tissue on fluid and solid mechanics in the vasculature [33].

References

[1] 1999, *Robbins Pathologic Basis of Disease*, R. S. Cotran, ed., Saunders, Philadelphia, PA.

[2] McGovern, P. G., Pankow, J. S., Shahar, E., Doliszny, K. M., Folsom, A. R., Blackburn, H., and Luepker, R. V., 1996, "Recent Trends in Acute Coronary Heart Disease—Mortality, Morbidity, Medical Care, and Risk Factors. The Minnesota Heart Survey Investigators," N. Engl. J. Med., **334**(14), pp. 884–890.

[3] Friedman, M. H., 2002, "Variability of 3D Arterial Geometry and Dynamics,

and Its Pathologic Implications," Biorheology, **39**(3–4), pp. 513–517.
[4] VanEpps, J. S., and Vorp, D. A., 2007, "Mechanopathobiology of Atherogenesis: A Review," J. Surg. Res., **142**(1), pp. 202–217.
[5] Asakura, T., and Karino, T., 1990, "Flow Patterns and Spatial Distribution of Atherosclerotic Lesions in Human Coronary Arteries," Circ. Res., **66**(4), pp. 1045–1066.
[6] Friedman, M. H., Bargeron, C. B., Deters, O. J., Hutchins, G. M., and Mark, F. F., 1987, "Correlation Between Wall Shear and Intimal Thickness at a Coronary Artery Branch," Atherosclerosis, **68**(1–2), pp. 27–33.
[7] Friedman, M. H., Hutchins, G. M., Bargeron, C. B., Deters, O. J., and Mark, F. F., 1981, "Correlation Between Intimal Thickness and Fluid Shear in Human Arteries," Atherosclerosis, **39**(3), pp. 425–436.
[8] Kornet, L., Lambregts, J., Hoeks, A. P., and Reneman, R. S., 1998, "Differences in Near-Wall Shear Rate in the Carotid Artery Within Subjects are Associated With Different Intima-Media Thicknesses," Arterioscler., Thromb., Vasc. Biol., **18**(12), pp. 1877–1884.
[9] Ku, D. N., Giddens, D. P., Zarins, C. K., and Glagov, S., 1985, "Pulsatile Flow and Atherosclerosis in the Human Carotid Bifurcation. Positive Correlation Between Plaque Location and Low Oscillating Shear Stress," Arteriosclerosis (Dallas), **5**(3), pp. 293–302.
[10] Zarins, C. K., Giddens, D. P., Bharadvaj, B. K., Sottiurai, V. S., Mabon, R. F., and Glagov, S., 1983, "Carotid Bifurcation Atherosclerosis. Quantitative Correlation of Plaque Localization With Flow Velocity Profiles and Wall Shear Stress," Circ. Res., **53**(4), pp. 502–514.
[11] Moore, J. E., Xu, C., Glagov, S., Zarins, C. K., and Ku, D. N., 1994, "Fluid Wall Shear Stress Measurements in a Model of the Human Abdominal Aorta: Oscillatory Behavior and Relationship to Atherosclerosis," Atherosclerosis, **110**(2), pp. 225–240.
[12] Stein, P. D., Hamid, M. S., Shivkumar, K., Davis, T. P., Khaja, F., and Henry, J. W., 1994, "Effects of Cyclic Flexion of Coronary Arteries on Progression of Atherosclerosis," Am. J. Cardiol., **73**(7), pp. 431–437.
[13] Thubrikar, M. J., Baker, J. W., and Nolan, S. P., 1988, "Inhibition of Atherosclerosis Associated With Reduction of Arterial Intramural Stress in Rabbits," Arteriosclerosis (Dallas), **8**(4), pp. 410–420.
[14] Thubrikar, M. J., Deck, J. D., Aouad, J., and Chen, J. M., 1985, "Intramural Stress as a Causative Factor in Atherosclerotic Lesions of the Aortic Valve," Atherosclerosis, **55**(3), pp. 299–311.
[15] Thubrikar, M. J., and Robicsek, F., 1995, "Pressure-Induced Arterial Wall Stress and Atherosclerosis," Ann. Thorac. Surg., **59**(6), pp. 1594–1603.
[16] Salzar, R. S., Thubrikar, M. J., and Eppink, R. T., 1995, "Pressure-Induced Mechanical Stress in the Carotid Artery Bifurcation: A Possible Correlation to Atherosclerosis," J. Biomech., **28**(11), pp. 1333–1340.
[17] Aikawa, M., Sivam, P. N., Kuro'o, M., Kimura, K., Nakahara, K., Takewaki, S., Ueda, M., Yamaguchi, H., Yazaki, Y., and Periasamy, M., 1993, "Human Smooth Muscle Myosin Heavy Chain Isoforms as Molecular Markers for Vascular Development and Atherosclerosis," Circ. Res., **73**(6), pp. 1000–1012.
[18] Ding, Z., and Friedman, M. H., 2000, "Dynamics of Human Coronary Arterial Motion and Its Potential Role in Coronary Atherogenesis," ASME J. Biomech. Eng., **122**(5), pp. 488–492.
[19] Ding, Z., Zhu, H., and Friedman, M. H., 2002, "Coronary Artery Dynamics In Vivo," Ann. Biomed. Eng., **30**(4), pp. 419–429.
[20] Gross, M. F., and Friedman, M. H., 1998, "Dynamics of Coronary Artery Curvature Obtained From Biplane Cineangiograms," J. Biomech., **31**(5), pp. 479–484.
[21] Hamid, M. S., Davis, T. P., and Stein, P. D., 1992, "Cyclic Flexion of the Coronary Arteries is a Possible Contributing Factor to Coronary Atherosclerosis," Adv. Bioeng., **22**, pp. 329–331.
[22] Pao, Y. C., Lu, J. T., and Ritman, E. L., 1992, "Bending and Twisting of an In Vivo Coronary Artery at a Bifurcation," J. Biomech., **25**(3), pp. 287–295.
[23] Lehoux, S., and Tedgui, A., 2003, "Cellular Mechanics and Gene Expression in Blood Vessels," J. Biomech., **36**(5), pp. 631–643.
[24] Lu, X., Yang, J., Zhao, J. B., Gregersen, H., and Kassab, G. S., 2003, "Shear Modulus of Porcine Coronary Artery: Contributions of Media and Adventitia," Am. J. Physiol. Heart Circ. Physiol., **285**(5), pp. H1966–H1975.
[25] Deng, S. X., Tomioka, J., Debes, J. C., and Fung, Y. C., 1994, "New Experiments on Shear Modulus of Elasticity of Arteries," Am. J. Physiol., **266**(1 Pt 2), pp. H1–H10.
[26] 1983, "What Principle Governs the Stress Distribution in Living Organisms," *Biomechanics in China, Japan, and USA*, Y. C. Fung, E. Fakada, and J. Wang, eds., Science, Beijing, pp. 1–13.
[27] Vaishnav, R. N., and Vossoughi, J., 1983, "Estimation of Residual Strains in Aortic Segments," *Biomechanical Engineering II, Recent Developments*, C. W. Hall, ed., Pergamon, New York, pp. 330–333.
[28] Humphrey, J. D., 2002, *Cardiovascular Solid Mechanics Cells, Tissues, and Organs*, Springer, New York.
[29] Chuong, C. J., and Fung, Y. C., 1983, "Three-Dimensional Stress Distribution in Arteries," ASME J. Biomech. Eng., **105**(3), pp. 268–274.
[30] Wang, C., Garcia, M., Lu, X., Lanir, Y., and Kassab, G. S., 2006, "Three-Dimensional Mechanical Properties of Porcine Coronary Arteries: A Validated Two-Layer Model," Am. J. Physiol. Heart Circ. Physiol., **291**(3), pp. H1200–H1209.
[31] Frobert, O., Gregersen, H., Bjerre, J., Bagger, J. P., and Kassab, G. S., 1998, "Relation Between Zero-Stress State and Branching Order of Porcine Left Coronary Arterial Tree," Am. J. Physiol., **275**(6 Pt 2), pp. H2283–H2290.
[32] Guo, X., and Kassab, G. S., 2004, "Distribution of Stress and Strain Along the Porcine Aorta and Coronary Arterial Tree," Am. J. Physiol. Heart Circ. Physiol., **286**(6), pp. H2361–H2368.
[33] Zhang, W., Herrera, C., Atluri, S. N., and Kassab, G. S., 2004, "Effect of Surrounding Tissue on Vessel Fluid and Solid Mechanics," ASME J. Biomech. Eng., **126**(6), pp. 760–769.